PCCP

PAPER

View Article Online
View Journal | View Issue

Cite this: *Phys. Chem. Chem. Phys.*, 2015, **17**, 2404

Effective targeting of proton transfer at ground and excited states of *ortho*-(2′-imidazolyl)naphthol constitutional isomers†

Thaís C. F. Oliveira,‡[a] Luiz F. V. Carmo,‡[a] Bárbara Murta,[a] Luís G.T.A. Duarte,[b] Rene A. Nome,[b] Willian R. Rocha*[a] and Tiago A. S. Brandão*[a]

Received 25th September 2014,
Accepted 19th November 2014

DOI: 10.1039/c4cp04337e

www.rsc.org/pccp

Steady-state and time-resolved spectroscopy and quantum chemical computational studies were employed to investigate ground and excited state proton transfer of a novel series of *ortho*-(1*H*-imidazol-2-yl)naphthol constitutional isomers: 1-(1*H*-imidazol-2-yl)naphthalen-2-ol (1NI2OH), 2-(1*H*-imidazol-2-yl)naphthalen-1-ol (2NI1OH) and 3-(1*H*-imidazol-2-yl)naphthalen-2-ol (3NI2OH). Proper Near Attack Conformations (NACs) involving a strong intramolecular hydrogen bond between the naphthol moiety and the *ortho*-imidazole group account for the highest ground state acidity of 2NI1OH compared with 1NI2OH and 3NI2OH. Moreover, ESIPT for 2NI1OH and 3NI2OH is further associated with planar chelate H-ring formation whereas 1NI2OH shows the highest ESIPT barrier and a noncoplanar imidazole group. In addition to energetic and structural requirements, the final state also depends on electronic configuration of the ESIPT product with the neutral 3NI2OH showing an ICT effect that correlates with the excited state pK_a of the cationic species.

Introduction

When two reactive groups are within a short distance of each other, bond formation occurs after a near attack conformation (NAC) is attained.[1] In the NAC, as previously proposed by the so-called spatiotemporal relationship,[2] the reacting atoms are tuned by a sufficient time with precise proximity and alignment structurally resembling the transition state (TS). These fundamental aspects have been used by chemists and biochemists in the design of enzyme models and understanding of enzyme efficiency.[3] In essence, intermolecular reactions have fewer NACs over time and are much slower than intramolecular or enzymatic reactions where proper NACs were selected.[1a,4]

We look for NACs in ground and excited state proton transfer reactions. Proper alignment and proximity are essential for efficient ground state proton transfer in many acid and base-catalyzed reactions in biology and chemistry,[5] including isomerization[3e,6] and functional group transfer.[7] Proton transfer is also a common photoinduced process for organic molecules showing enhanced excited state acidity or basicity.[8] Common acidic groups in the excited-state are phenolic OH,[8a,d] whereas basic sites are usually heteroatoms like a carbonyl oxygen or heterocyclic nitrogen.[8a,9] While bimolecular proton transfer is driven by solvent dynamics,[8a,10] excited state intramolecular proton transfer (ESIPT) may occur when the acidic and basic sites are in proximity.[8a,c,e] ESIPT has attracted attention for its fundamental nature and potential for chemical and biological applications (*e.g.* sensing, pH-jumps, and photoswitches).[8e,11] Intramolecular proton transfer reactions occur on adiabatic potential energy surfaces and thus both ground and excited state reactions can in principle be understood on the same footing.

In this paper, we investigate ground and excited state proton transfer in three *ortho*-(1*H*-imidazol-2-yl)naphthol constitutional isomers termed 1NI2OH, 2NI1OH and 3NI2OH based on the naphthalene ring position of an acidic OH and a basic imidazole group (Scheme 1). Naphthalene is a rigid carbon framework, luminescent and allows two distinct *ortho* substitutions (1,2 and 2,3) with different structural effects that may either improve or impair the occurrence of intramolecular proton transfer reactions. Thus, the naphthalene skeleton offers a valuable tool for the study of spatiotemporal effects on proton transfer and hydrogen bonding at the ground and excited states.

A strong intramolecular hydrogen bond (IMHB) between the acidic OH and basic imidazole group is the driving force to obtain NACs in proton transfer. However, geometric restraints

[a] *Department of Chemistry, ICEX, Federal University of Minas Gerais, Belo Horizonte, MG, 31270-901, Brazil. E-mail: wrocha@ufmg.br, tasb@ufmg.br; Fax: +55 31 3409-5700; Tel: +55 31 3409-5766*
[b] *Institute of Chemistry, State University of Campinas, Campinas, SP, 13083-970, Brazil*

† Electronic supplementary information (ESI) available: Synthetic procedures and characterization data for all synthesized compounds. Spectroscopic data for all pH-titrations and for different solvents. Selected structures at the PES of Fig. S5. HOMO and LUMO orbitals diagrams for computationally optimized structures in Fig. S4 and their Cartesian coordinates. See DOI: 10.1039/c4cp04337e

‡ T.C.F.O. and L.F.V.C. contributed equally to this work.

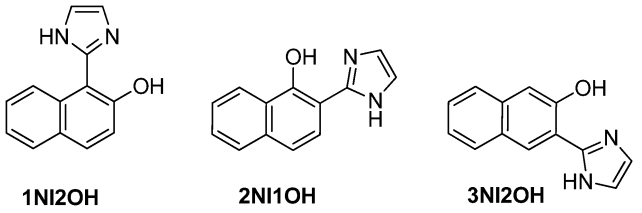

Scheme 1 Constitutional isomers of *ortho*-(1*H*-imidazol-2-yl)naphthol studied in this work.

may prevent free movement of these two groups and a balance between electronic and geometric effects should be considered for proper NAC. Effective targeting means designing molecules with specific electronic and structural features that lead to an increase of NAC concentration thereby resulting in more efficient reactions. Such an increase in NAC concentration has been related to a higher effective molarity of reactants in intramolecular reactions when compared with the corresponding intermolecular ones. For example, in the context of ground and excited state intramolecular proton transfer, effective targeting means tuning the molecular structure to optimize the donor–acceptor distance, which is the proton transfer reaction coordinate. Supported by experimental and theoretical studies, we show that each *ortho*-(1*H*-imidazol-2-yl)naphthol isomer exhibits distinct geometric and electronic requirements affecting ground and excited state intramolecular proton transfer. It shall be noted that the imidazole group mimics the role of histidine residues in proton transfer reactions in proteins which plays an important role in the ground state of general-acid or general-base catalysts. However, it has been marginally considered at the excited state of biological processes despite many examples of ESIPT processes in small molecules.[12]

Results and discussion

Based on the computational and spectroscopic data presented in this article as well as related work with imidazole,[12a,b,13] benzimidazoles[12c–g,14] and imidazopyridines,[15] Schemes 2 and 3 provide a framework for analysis of proton transfer in the three *ortho*-(1*H*-imidazol-2-yl)naphthol isomers studied here. Scheme 2 shows acid–base equilibria for the ground and excited state. Depending on experimental conditions, each chemical species in Scheme 2 may involve several conformers originated from tautomerism, rotamerism and solvent interaction. Scheme 3 provides the species showing IMHBs and those related to ground and excited state intramolecular proton transfer. The N_{anti} and N_{syn} forms in equilibrium with each other differ on IMHB formation with the imidazole group as the HB donor and acceptor, respectively.[16]

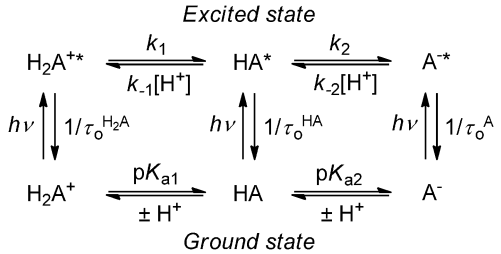

Scheme 2 Proton equilibria at ground and excited states for *ortho*-(1*H*-imidazol-2-yl)naphthols. The pK_{a1}* and pK_{a2}* represents $-\log(k_{forward}/k_{reverse})$.

For H_2A^+ species a hydrogen bond between the phenol and the imidazolium group is expected to give the N_{anti} species as the only one showing IMHBs. However, the HA species exhibits complex equilibria. Interannular bond rotation in S_0-N_{anti} gives the S_0-N_{syn} form with the imidazole group as a HB acceptor. In the excited state, the S_1-N_{syn} form undergoes an ESIPT reaction to give Proton Transferred (PT) species depending on the IMHB strength. Thus, ESIPT is likely to occur whenever the excited state phenol is a stronger acid than the base's conjugated acid in the S_1-N_{syn} species. The S_1-PT species formally exists as two rotamers, S_1-T_{syn} and S_1-T_{ICT}, which represent a twisted intramolecular charge transfer (TICT) state with interannular bond rotation and nonplanar configuration of the naphthalene and imidazole rings. S_1-PT emission is followed by favorable ground state intramolecular proton transfer (GSIPT) from the S_0-PT to S_0-N_{syn} form. The A^- species in solution assumes the N_{anti} form, which does not undergo proton transfer in water until pH 12.

Fig. 1 depicts steady-state absorption (UV-Vis) and emission (fluorescence) spectra for 1NI2OH, 2NI1OH and 3NI2OH at different pH values in aqueous solutions at 25 °C. From pH 2 to 12, the spectroscopic data (refer to Fig. S10–S15 in the ESI† for the full data set) is consistent with the diprotic acid–base equilibria shown in Scheme 2. In order to refer to different species in the text, we consider the compound notation superscripted by the overall charge species, *e.g.*, $1NI2OH^+$, $1NI2OH^n$ and $1NI2OH^-$ refer to the respective H_2A^+, HA and A^- species. Table 1 gives ground state acidity constants (pK_a) determined from fluorescence intensity titrations, which afford pK_a values quite similar to those obtained from UV-Vis titrations (see Table 1 footnote). Table 1 also presents excited state pK_a values determined from fluorescence lifetime titrations in the 0.01 to 8 M HCl concentration range (see below). Fig. 1 presents spectra measured at pH values close to the highest concentration of each species in the ground state. Table 2 presents quantum yields for each species and the respective maximum emission wavelength along with decay constants from fluorescence lifetime measurements.

Absorption studies

π,π* transitions dominate the absorption spectra of 1NI2OH, 2NI1OH and 3NI2OH, with molar absorptivities and maximum absorption wavelength influenced by both position and conformation of groups attached to the naphthalene ring. According to Platt's theory,[17] the lowest excited state for ^1A to ^1L transitions in naphthalene is polarized along the long molecular axis (L_b) whereas the short molecular axis (L_a) exhibits larger polarity and energy (Fig. 2). The ^1A–^1L_a and ^1A–^1L_b transitions for *ortho*-(1*H*-imidazol-2-yl)naphthol isomers studied here are respectively observed at 230–280 nm ($\log \varepsilon \sim 4.5$ for neutral species) and 330–390 nm ($\log \varepsilon \sim 3.7$ for neutral species). Taking this into account and the substitution pattern of 1NI2OH, 2NI1OH and 3NI2OH, intramolecular hydrogen bonding and acid–base equilibria

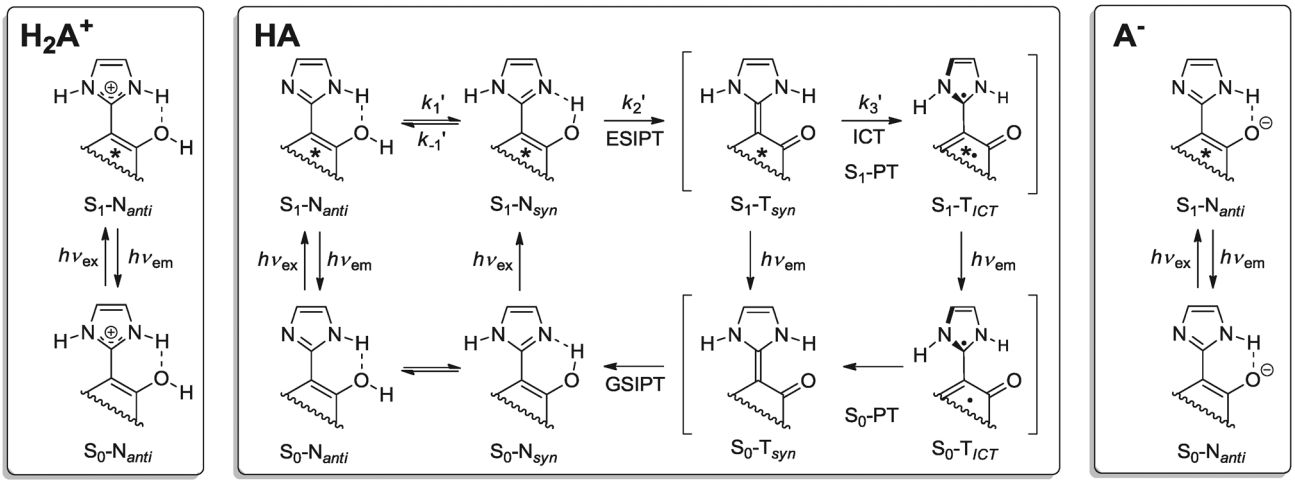

Scheme 3 Structures of various ground and excited state acid–base species for *ortho*-(1*H*-imidazol-2-yl)naphthol constitutional isomers. H_2A^+, HA and A^- are the cationic, neutral and anionic species, respectively.

involving substituents at the alpha (C1) are expected to affect the ^1A–^1L_a transition, while the ^1A–^1L_b transition responds to groups at the beta (C2) position. Therefore, hydroxyl group deprotonation at the beta position is more evident for 1NI2OH than 2NI1OH, as observed by spectroscopic changes near 350 nm in Fig. 1. Similar analysis has been provided for *ortho*-hydroxynaphthoic acids[18] and their esters.[19] Next, we focus on the stereoelectronic relationship between the vicinal imidazole and hydroxyl groups in 1NI2OH and 2NI1OH, which provide an orthogonal analysis for structural effects in the ground state.

The imidazole group at the alpha position of the naphthalene ring of 1NI2OH is non-coplanar for steric reasons and shows absorption bands at 331 and 332 nm for $1NI2OH^+$ and $1NI2OH^n$ species, respectively. The shoulder at 356 nm for $1NI2OH^n$ preludes full naphthol deprotonation and suggests the existence of IMHBs between the neutral imidazole and the naphthol group. This conclusion is based on the fact that $1NI2OH^n$ deprotonation to $1NI2OH^-$ has a hyperchromic effect at 356 nm due to aryloxide group conjugation with the naphthalene ring. Significant red-shift and hyperchromic effects are also observed at 230–250 nm (the L_a axis), an indication that the neutral imidazole group is involved in IMHB interaction in the $1NI2OH^-$ species (refer to Fig. S10 in the ESI†). This six membered-ring interaction involves the NH imidazole moiety and the aryloxide group in a coplanar configuration, in which the H-8 naphthalene ring and the imidazole nitrogen atom sp^2 lone pair form a *peri*-interaction as proposed for related naphthalene compounds (Scheme 4).[19,20]

The deprotonation of species $2NI1OH^+$ to $2NI1OH^n$ involves a bathochromic shift and a hyperchromic effect (at the L_b axis) associated with increasing conjugation – at near coplanarity – between the imidazole moiety and the naphthalene ring, thus leading to strong IMHB between the neutral imidazole (HB acceptor) and the hydroxyl group (HB donor) in $2NI1OH^n$. Therefore, due to this interaction a substantial change is also observed at 230–250 nm (the L_a axis). Because this IMHB is strong, deprotonation of species $2NI1OH^n$ to form $2NI1OH^-$ occurs only with a small influence over ^1A–^1L_a, and a small blue shift in absorption maximum along the L_b axis.

The imidazole and hydroxyl groups in 3NI2OH are positioned at the long molecular axis (L_b) and deprotonation of $3NI2OH^+$ and $3NI2OH^n$ has little effect at 230–250 nm (the L_a axis).

Fluorescence studies

Table 2 summarizes steady-state and time-resolved fluorescence spectroscopy data for 1NI2OH, 2NI1OH and 3NI2OH in water from pH 2 to 12. In the steady-state studies, the excitation wavelength for each compound was chosen to provide similar absorption contributions for individual ground state species (Fig. 1). However, the excitation wavelengths do not represent isoabsorption points, which we do not take as critical for all comparisons since emission contributions may differ for each species. Thus, we base our discussion on the observed quantum yield, which takes into account the ratio of emitted to absorbed photons. The emission spectra represent $S_1 \rightarrow S_0$ transitions influenced by position and proximity between hydroxyl and imidazole groups, including the various conformers shown in Scheme 3. Thus, fluorescence spectra report on ground and excited state species distribution whereas lifetime depends upon excited state structure. As summarized in Table 1, species distribution may differ for both electronic states depending on the functional group attached to the naphthalene ring. For example, the pK_a for 1- and 2-naphthols and their derivatives always decrease at the excited state.[8d,21] pK_a* values for 2-naphthol compounds substituted with electron-withdrawing groups or showing ESIPT are usually lower than 2.8 (the pK_a* for 2-naphthol);[8d,9,22] the respective ground state pK_a for 2-naphthol is 9.3. Heterocyclic amines such as acridine exhibit higher excited state basicity with pK_a* values for the conjugated acid about 5 units above the corresponding ground state pK_a.[8a,9] By contrast, the imidazole moiety in 2-(2′-hydroxyphenyl)benzimidazole does not undergo any increase in basicity upon photo-excitation,[23] and 1*H*-imidazol-5-yl-vinyl

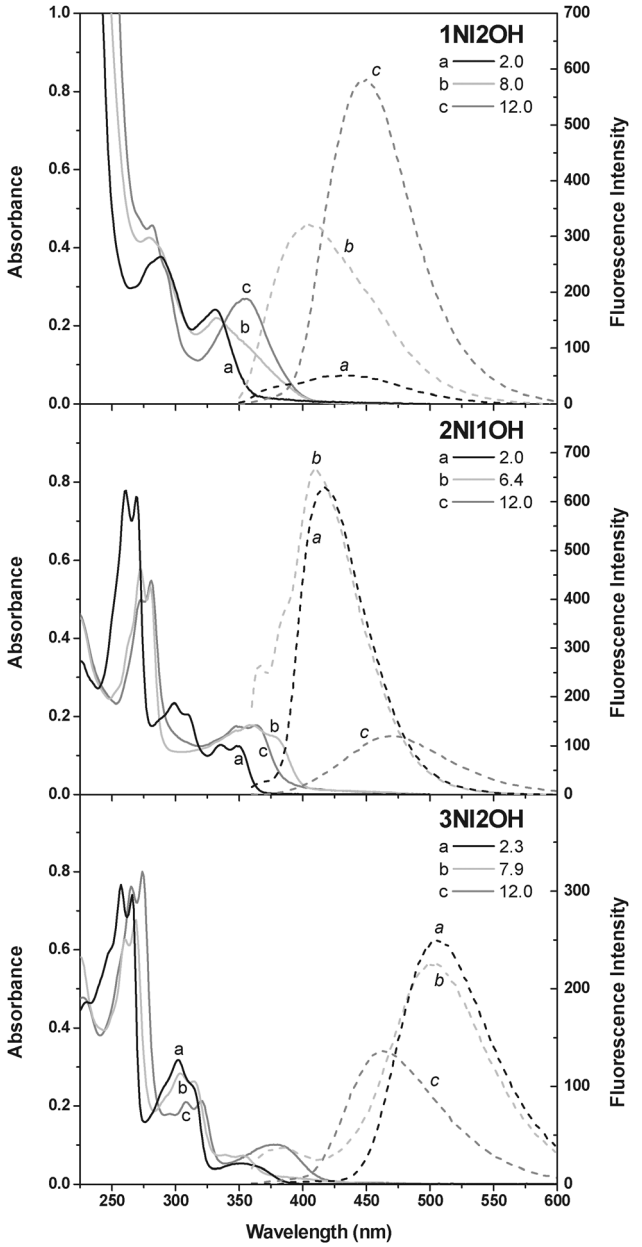

Fig. 1 Absorption (solid line) and emission (broken line) spectra for 1-(1*H*-imidazol-2-yl)naphthalen-2-ol (1NI2OH, 5.96×10^{-5} M), 2-(1*H*-imidazol-2-yl)naphthalen-1-ol (2NI1OH, 2×10^{-5} M) and 3-(1*H*-imidazol-2-yl)naphthalen-2-ol (3NI2OH, 2×10^{-5} M) in water at the indicated pH values and 25 °C. The excitation wavelength for 1NI2OH was 330 nm and for 2NI1OH and 3NI2OH it was 350 nm.

derivatives in the excited state show a drop of 1.4 pK_a units for the imidazolium moiety.[24]

Excitation of $1NI2OH^+$ at pH 2.0 gives a weak and broad emission band with a maximum wavelength near 435 nm. Compared with higher pH values, the low quantum yield at pH 2 (Φ_{obs} = 0.024) indicates that the $S_1 \rightarrow S_0$ emission of $1NI2OH^+$ competes with nonradiative decay paths provided by vibronic effects of the noncoplanar imidazolium group and naphthol group deprotonation to afford PT species. The pK_a* of all three H_2A^+ *ortho*-(1*H*-imidazol-2-yl)naphthol species are

Table 1 Acidity constants for 1NI2OH, 2NI1OH and 3NI2OH in aqueous solutions and strong acidic conditions at 25 °C[a]

Parameters	1NI2OH	2NI1OH	3NI2OH
pK_{a1}	6.68 ± 0.01	4.24 ± 0.01	6.47 ± 0.01
pK_{a2}	9.73 ± 0.01	8.71 ± 0.01	9.35 ± 0.01
pK_{a1}* [b,c]	−0.60 ± 0.13[d]	−0.95 ± 0.01	−1.70 ± 0.03

[a] The respective pK_{a1} and pK_{a2} values determined using UV-Vis spectroscopy were: 6.87 ± 0.01 and 9.59 ± 0.01 for 1NI2OH, 4.22 ± 0.03 and 8.50 ± 0.02 for 2NI1OH, and 6.51 ± 0.02 and 9.23 ± 0.01 for 3NI2OH. [b] Based on the H_0-fluorescence lifetime profile. [c] The H_0-inflection values determined from the H_0-dependence of fluorescence intensities were −0.58 ± 0.04 for 1NI2OH, −0.96 ± 0.01 for 2NI1OH, and −0.89 ± 0.01 for 3NI2OH. A second H_0-inflection at −2.33 ± 0.04 was found for 1NI2OH and assigned to a dication species. [d] Average for the pK_{a1}* of −0.60 ± 0.13 and −0.59 ± 0.13 determined from the H_0-fluorescence lifetime profiles at 0.5 to 1.0 ns and 2.4 to 3.2 ns, respectively.

Table 2 Maximum absorption and emission wavelengths, quantum yields and emission lifetime for 1NI2OH, 2NI1OH and 3NI2OH species in aqueous solutions at 25 °C

Parameters	λ_{max}[a] (abs) $S_0 \rightarrow S_1$	λ_{max} (em) $S_1 \rightarrow S_0$	Φ_{obs}[b]	τ[b,c] (ns)
$1NI2OH^+$ (H_0 −3.8)	331	395	n.d.	0.5; 3.1
$1NI2OH^+$ (pH 2.0)	331	435	0.024	0.6; 2.8
$1NI2OH^n$ (pH 8.0)	332 (*356*)	405	0.14	1.6; 4.4
$1NI2OH^-$ (pH 12.0)	355	450	0.32	3.6
$2NI1OH^+$ (H_0 −3.8)	350	386	n.d.	2.9
$2NI1OH^+$ (pH 2.0)	349	417	0.20	1.3
$2NI1OH^n$ (pH 6.4)	359 (*375*)	410	0.18	1.3
$2NI1OH^-$ (pH 12.0)	364	470	0.043	4.0
$3NI2OH^+$ (H_0 −3.8)	351	417	n.d.	6.2
$3NI2OH^+$ (pH 2.3)	351	507	0.25	9.0
$3NI2OH^n$ (pH 7.9)	352 (*393*)	502	0.18	3.2; 9.1
$3NI2OH^-$ (pH 12.0)	378	462	0.12	2.1; 7.0

[a] Shoulders are shown in italic between parenthesis. [b] Standard deviations for the last decimal place are lower than unity. [c] Values separated by semicolon were taken from biexponential fluorescence decays.

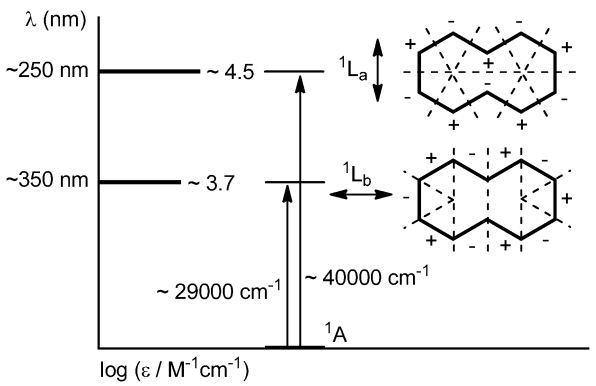

Fig. 2 Electronic energy levels of naphthalene and polarization diagrams for low absorption bands. Energies and log ε are averages of measurements for the neutral species of *ortho*-(1*H*-imidazol-2-yl)naphthols.

below zero and observed under very acidic media ([HCl] > 0.01 M) (*vide infra*). Therefore, for pH > pK_a* a small concentration of $1NI2OH^+$ is assumed at equilibrium. Emission from the PT species

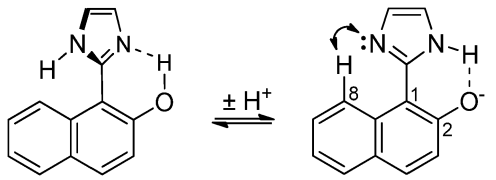

Scheme 4 IMHB interactions on 1NI2OH^n and 1NI2OH$^-$ species.

is likely to occur at longer wavelengths when compared with emission from 1NI2OH$^+$. The broad emission band from 1NI2OH$^+$ exhibits a shoulder at 395 nm (a band at HCl > 0.5 M, *vide infra*) and maximum wavelength near 435 nm, which we suggest to be respective contributions of S_1-N_{anti} for 1NI2OH$^+$ and S_1-PT for 1NI2OH^n.

As shown above, excitation of 1NI2OH^n at pH 8.0 also presents a broad and stronger emission band (Φ_{obs} = 0.14) formed by two different components emitting near 385 and 455 nm, which we assign to the emission from S_1-N_{anti} and S_1-PT forms, respectively. This assignment is consistent with the presence of two bands in the fluorescence spectrum of 1NI2OH in three different solvents: methanol, ethanol 95%, and, particularly, acetonitrile, a solvent in which ESIPT occurs without competing acid–base equilibria or proton transfer to the solvent (refer to Fig. S19 in the ESI†).

Two main reasons may be claimed to account for the stronger emission of S_1-PT at pH 8.0 relative to more acidic conditions: (i) $1/\tau_o^{HA} \gg k_{-1}$ [H$^+$] at low acid concentration; (ii) excited state intramolecular proton transfer (ESIPT) in 1NI2OH^n is comparatively faster than bimolecular proton transfer from 1NI2OH$^+$ to water. All observations above are in agreement with lifetime measurements. 1NI2OH time-resolved emission at pH 2.0 and 8.0 fit in both cases to biexponential rate equations, indicating the existence of two species in solution. We propose that S_1-PT species are long-lived compared with S_1-N_{anti}. This assumption follows the corresponding observations for 2-(2′-hydroxyphenyl)-benzimidazole (HBI) and studies of the contribution of the decay components (α) in different emission wavelengths. In pH 8.0 the short-lived S_1-N_{anti} contribution is higher at short wavelengths (α_1 = 0.039 at 410 nm and 0.017 at 460 nm) while the long-lived S_1-PT species presents the opposite behavior (α_2 = 0.003 at 410 nm and 0.005 at 460 nm).[12b,14]

Excitation of 1NI2OH$^-$ (at pH 12.0) gives a single and intense band (Φ_{obs} = 0.32) with maximum wavelength at 450 nm and a monoexponential decay with τ of 3.6 ns. Compared with lower pHs, higher Φ_{obs} and τ are indicative of an IMHB interaction between aryloxide and neutral imidazole due to coplanarity and diminishing vibronic effects that could affect radiative decay.

Excitation of the cationic species of 2NI1OH (at pH 2.0) and of 3NI2OH (at pH 2.3) give in both cases single and strong emission bands respectively at 417 and 507 nm, which can be rationalized as contributions of S_1-PT species. Emission contributions in both cases are associated to single species showing single exponential decays with respective τ values of 1.3 and 9.1 ns to 2NI1OH and 3NI2OH.

The emission spectra for neutral species of 2NI1OH (at pH 6.4) and 3NI2OH (at pH 7.9) are similar to the spectra observed near pH 2.0, except for blue-shifted emissions for S_1-N_{anti} forms when k_{-1}[H$^+$] ≪ $1/\tau_o^{HA}$. In each case, bands near neutrality exhibit contributions from two different components emitting near 410 and 440 nm for 2NI1OH and 380 and 500 nm for 3NI2OH. These observations are in agreement with measurements in different solvents (refer to Fig. S19 in the ESI†) showing two characteristic emission bands for S_1-N_{anti} and S_1-PT species in going from water to acetonitrile. Consistently, the emission behavior of 3NI2OH at pH 7.9 shows a biexponential decay with τ values of 3.2 and 9.1 ns that we assume to represent respective contributions of S_1-N_{anti} and S_1-PT forms. This assignment agrees with analysis of the contribution of decay components, which is higher at short wavelengths for the short-lived S_1-N_{anti} (α_1 = 0.058 at 460 nm and 0.016 at 500 nm) compared to the long-lived S_1-PT (α_2 = 0.016 at 460 nm and 0.048 at 500 nm). As one may expect, the slower decay of 9.1 ns is also observed at pH 2.0 where the S_1-N_{anti} is not observed. However, monoexponential decay with a τ value of 1.3 ns for S_1-N_{anti} species contribution was obtained for 2NI1OH at pH 6.4, which the S_1-PT decay with a longer lifetime was undetected owing to the fast equilibrium with S_1-N_{anti} showing preferential radiative decay.

Large differences between the emission spectra for the excitation of the anionic species of 2NI1OH and 3NI2OH (both at pH 12.0) and the emission spectra under neutral or acidic conditions are indicative that fluorescence emission belongs to different species. The emission band for 2NI1OH$^-$ is observed at higher wavelengths (at 470 nm) and shows a low observed quantum yield (Φ_{obs} = 0.043) owing to nonradiative decay that may involve solvent and vibronic effects. The emission band for 3NI2OH$^-$ is also less intense, but observed at lower wavelengths (at 462 nm, Φ_{obs} = 0.12) in relation to 3NI2OH S_1-PT species with large ICT effects.

Spectroscopic titrations

The acidity constants (pK_a) in Table 1 were calculated using the computer program SQUAD[25] and spectroscopic data taken at different pH values from near 2 to 12. SQUAD is designed for executing calculations of the best stability constant values, individual spectra of species and speciation diagrams based on a proposed model (refer to Fig. S10–S15 in the ESI† for these results). Calculations were carried out minimizing the sum of square residuals of absorbance and fluorescence intensity values as a function of wavelength under different pH conditions.

As can be seen in Table 1, 2NI1OH presents significantly lower pK_a values compared with 1NI2OH and 3NI2OH, which have similar acidities in agreement with previous determinations for related 2-(1*H*-imidazol-2-yl)phenol; pK_{a1} = 6.5 (imidazolium) and pK_{a2} = 9.32 (phenol).[26] In this case, pK_a values reflect normal effects for a slight increase in the acidity of the imidazolium moiety, as observed for 2-phenylimidazolium with a pK_a of 6.4 related to imidazolium (pK_a = 7.0), and a 0.7 pK_a unit decrease for the phenol moiety compared with phenol alone (pK_a = 10.0).[27] The respective pK_a values for 1- and 2-naphthol are 9.42 and 9.57, close to values observed for 1NI2OH and 3NI2OH. These observations can be explained by electronic effects, but seemingly too small to claim any special structural effect. Nonetheless, despite the structural similarity

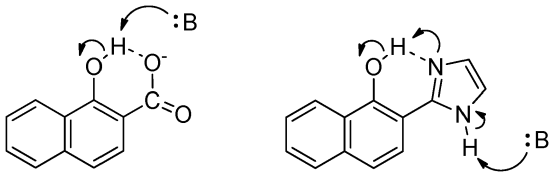

Scheme 5 Deprotonation reaction paths for 1-hydroxy-2-naphthoate and the HA species of 2NI1OH.

between 2NI1OH and its constitutional isomers 1NI2OH and 3NI2OH, the large pK_a difference of about 2.5 and 0.9 pK_a units for the respective imidazolium and phenol groups among these compounds undoubtedly requires a special structural effect at the ground state. A strong IMHB between imidazole and phenol largely stabilizes the HA species of 2NI1OH by about 14 kJ mol^{-1} ($\Delta\Delta G^\circ$ at 25 °C)[28] favoring the proton dissociation of H_2A^+.

In general, a strong IMHB makes the phenol less acidic as observed for salicylate[27] and 1-hydroxy-2-naphthoate,[4,29] which exhibit pK_a values near 13.0 and implies proton sponge behavior. The corresponding pK_a in 2-hydroxy-1-naphthoic acid – bearing a noncoplanar carboxylate moiety – is 9.83 consistent with negligible IMHBs. Indeed, this is very likely the only picture for the effect of a strong IMHB on the acidity of isolated phenol; however, since 2NI1OH deprotonation from HA to A^- may occur through another possible pathway involving the imidazole moiety (Scheme 5), IMHB has the opposite effect on acidity.

Based on the large effect on the pK_a values of 2NI1OH, it can be assumed that the IMHB is more efficiently tuned (at the ground state) for 2NI1OH compared with its constitutional isomers 1NI2OH and 3NI2OH. The spatiotemporal relationship in 2NI1OH^n is favored because periplanar hindrance impairs free rotation around the C–O bond, thus increasing the population of conformers favoring IMHBs as shown in Scheme 5. Similar structural observations were made to explain results from hydrolysis of *ortho*-acetoxy-naphthoic acetyl esters.[4] The same effect is not observed for neither 3NI2OH that exhibits groups with unhindered rotation nor for 1NI2OH where the periplanar effect weakens IMHBs due to the improper position assumed by the imidazole moiety.

SQUAD analysis of the fluorescence intensity data for 2NI1OH considering a diprotic acid–base equilibrium model as used for the absorption data gave quite poor results with substantial standard deviations. Conversely, the effect of pH on fluorescence intensities was in good agreement with three acid–base equilibria, two equilibria related to the ground state (pK_{a1} = 4.24 and pK_{a2} = 8.71) and a third one associated with the excited state with an inflection point at pH 5.47. Additional equilibrium studies are needed in order to assign the identity of this photochemical event, which very likely is related to acid dissociation of H_2A^+ to afford the HA species.

Fluorimetric studies in strong acidic media

As shown in Fig. 3, these studies were carried out by steady-state and time-resolved measurements employing HCl concentrations ranging from 0.01 to 8 M (pH 2 to H_0 −3.78).[30] Fig. 3b shows individual fluorescence decay profiles and the inserts show fluorescence lifetime as a function of pH (H_0 for [HCl] > 1 M) for each isomer. The smooth lines through the lifetime *vs.* pH data were calculated by nonlinear least square fitting using eqn (1), which takes into account lifetime molar fraction (χ) contributions of each species to the observed fluorescence lifetime (τ_{obs}). The calculated pK_{a1}* values are presented in Table 1 and the limiting τ values are shown on the top of each curve in the inserts of Fig. 3b.

$$\tau_{obs} = \tau_{H_2A^{+*}}\chi_{H_2A^{+*}} + \tau_{HA^*}\chi_{HA^*} \quad (1)$$

1NI2OH exhibits biexponential decay and the individual lifetime data were divided into two different sets that provided similar pK_{a1}* values of −0.60 and −0.59 for H_0-fluorescence lifetime profiles respectively at 0.5 to 1.0 ns and 2.4 to 3.2 ns. The identity between these pK_{a1}* values is indicative that the lifetime associated species in the two sets are related to the same equilibrium. Therefore, the average value of −0.60 was taken as the best estimate for the 1NI2OH$^+$ excited state acid dissociation constant. Fluorescence decays for 2NI1OH and 3NI2OH are all single exponential curves from pH 2 to H_0 −3.78 and fit well to eqn (1) with respective pK_{a1}* values of −0.95 and −1.70. Both pK_a* values are lower than determined for 1-naphthol (pK_a* = 0.5)[21b] and 2-naphthol (pK_a* = 2.8).[21a]

Fluorescence intensities at selected wavelengths are shown in the inserts of Fig. 3a as a function of pH or H_0 (for [HCl] > 1 M). The smooth lines are nonlinear least square fits according to eqn (2), which considers individual contributions of fluorescence intensities of the species and their molar fractions (χ) to the observed fluorescence intensity (F_{obs}). It shall be noted that the contribution of $\chi_{H_3A^{2+*}}$ is null for 2NI1OH and 3NI2OH, and because the absorption spectra do not vary appreciably below pH 2 for all compounds, the H_0-dependences for the fluorescence intensities on Fig. 3a are only related to excited state speciation.

$$F_{obs} = F_{H_3A^{2+*}}\chi_{H_3A^{2+*}} + F_{H_2A^{+*}}\chi_{H_2A^{+*}} + F_{HA^*}\chi_{HA^*} \quad (2)$$

H_0-inflection points for the lifetime *vs.* pH data shown in Fig. 3b are observed H_0 values of −0.58, −0.96, and −0.89 respectively for 1NI2OH, 2NI1OH, and 3NI2OH. Considering eqn (3)[9] and the limiting τ values shown in the inserts of Fig. 3b, the respective pK_a* values of −0.80, −0.61 and −1.05 were calculated for 1NI2OH, 2NI1OH, and 3NI2OH, in good agreement with values determined from H_0-fluorescence lifetime measurements (Table 1). A second and lower inflection point for 1NI2OH is found at H_0 −2.33, which may correspond to protonation of 1NI2OH$^+$ to a dication species. This protonation was not seen for 2NI1OH and 3NI2OH, but it has been recognized for 2-(*ortho*-hydroxyphenyl)benzimidazoles in very acidic conditions.[31]

$$H_0 = pK_{a^*} - \log(\tau_{H_2A^{+*}}/\tau_{HA^*}) \quad (3)$$

Although determination of accurate pK_a* values is quite demanding and comparison between different classes of compounds can be quite misleading, examples for particular compounds

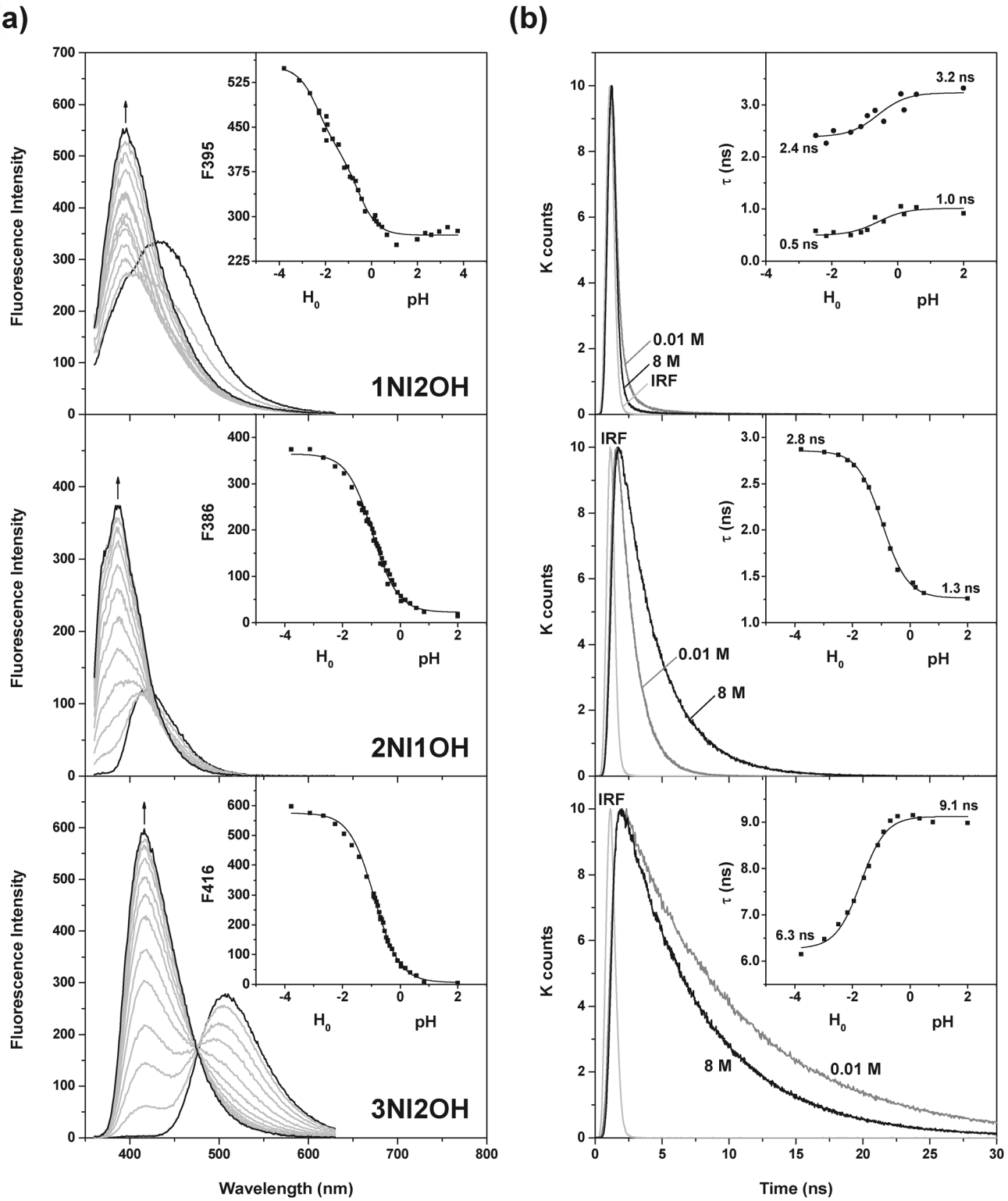

Fig. 3 Fluorimetric titrations in water from [HCl] 0.01 to 8 M at 25 °C for 1-(1*H*-imidazol-2-yl)naphthalen-2-ol (1NI2OH, 3×10^{-5} M), 2-(1*H*-imidazol-2-yl)naphthalen-1-ol (2NI1OH, 3×10^{-5} M) and 3-(1*H*-imidazol-2-yl)naphthalen-2-ol (3NI2OH, 2×10^{-5} M). (a) Emission spectra at λ_{ex} of 330 nm for 1NI2OH and 350 nm for 2NI1OH and 3NI2OH. Inserts show the pH/H_0-dependence of the fluorescence intensities (*F*) at the wavelengths indicated by the arrows. The solid lines are fits according to eqn (2); (b) fluorescence decays and instrumental response functions (IRF) profiles for representative measurements at λ_{ex} of 330 nm using the respective λ_{em} of 450, 400 and 462 nm for 1NI2OH, 2NI1OH and 3NI2OH. The inserts show pH/H_0-dependence of the lifetime. The solid lines were obtained from nonlinear least-square fit using the eqn (1) and the limiting τ values shown in the graphs. The value at pH 2 for 1NI2OH was taken as the average of measurements at pH 2.0, 4.0 and 8.0.

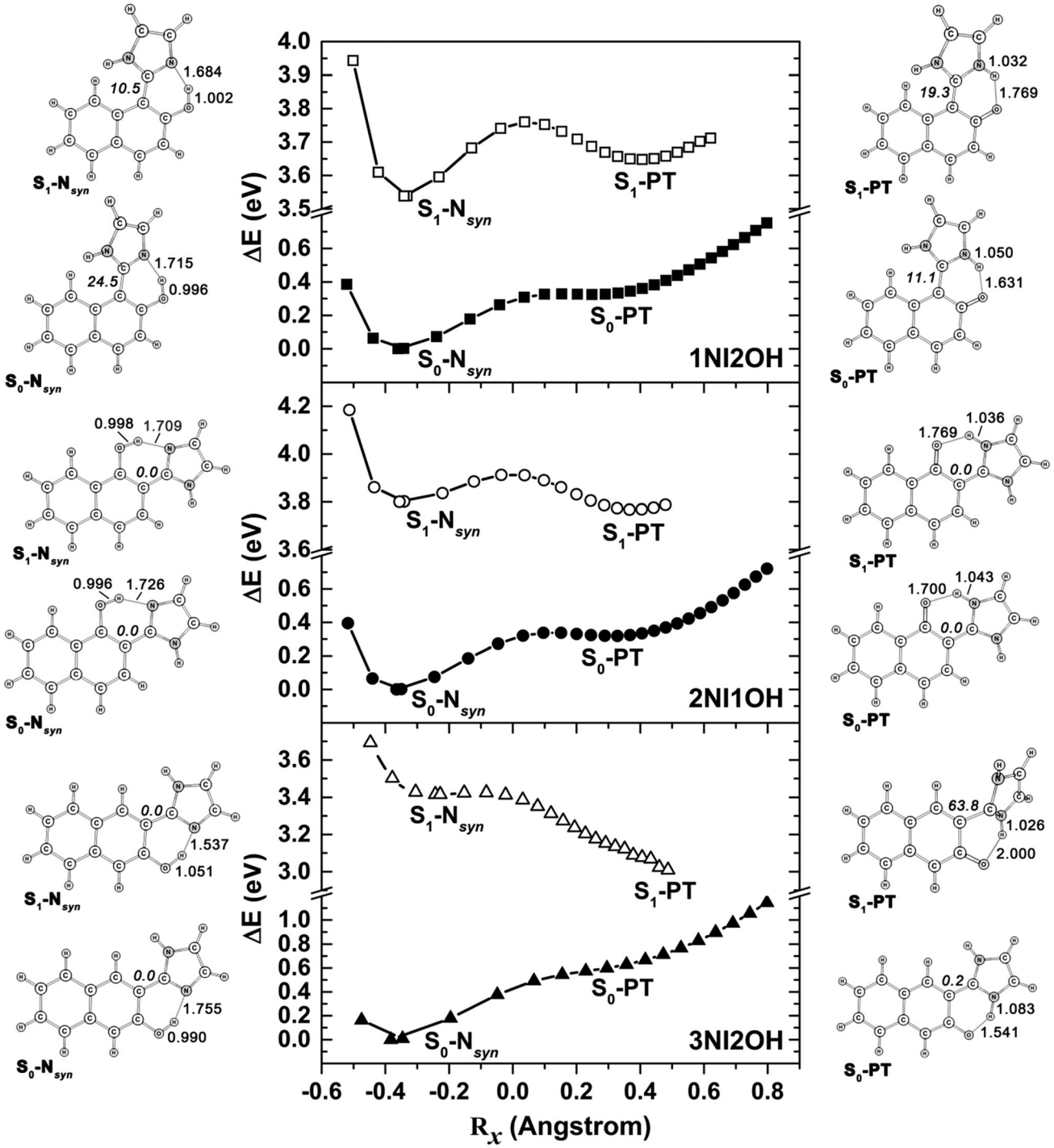

Fig. 4 Potential energy surface for the proton transfer in the ground state (S_0) and first (S_1) π,π^* excited state of 1NI2OH, 2NI1OH and 3NI2OH, and the corresponding structures for the N_{syn} and the PT forms of either S_0 or S_1 states. The bond lengths for O–H (in N_{syn}), N–H (in PT) and IMHBs are shown in angstroms, while the torsional angle for the interannular bond between the naphthol and the imidazole ring is shown in italic and degrees.

are found in the literature for Hammett-type correlations of the effect of different substituents on pK_a* values.[9,32] The structural similarity between 1NI2OH, 2NI1OH, and 3NI2OH encourages us to discuss differing pK_a* values seen in Table 1. 3NI2OH shows an unrestrained structure for coplanarity between imidazole and naphthol and presents higher acidity relative to 1NI2OH, in which the imidazole group is noncoplanar for steric reasons. Indeed, the photochemical behavior of 1NI2OH with two excited state species clearly indicates that ESIPT is quite disfavored. Geometric requirements impair the occurrence of an IMHB in the 1NI2OH H_2A^{+}* species which in turn may be responsible for the stronger acidity of 3NI2OH. Also, S_1-PT species of HA* species may be stabilized by IMHB with the same effect on the acid–base equilibrium. Another effect on the acidity of the *ortho*-(1*H*-imidazol-2-yl)naphthols may

Table 3 Computed energy variations (in kJ mol^{-1}) for the proton transfer reactions in the ground and excited states of the *ortho*-(1*H*-imidazol-2-yl)naphthols. Values between parentheses indicate the percentage of activation energy ($\Delta E^{\ddagger}$) decrease from ground to excited state

	Ground state		Excited state	
Compound	$\Delta E^{\ddagger}$	ΔE	$\Delta E^{\ddagger}$	ΔE
1NI2OH	31.4	31.4	21.4 (32%)	10.8
2NI1OH	32.6	30.8	10.8 (66%)	−3.22
3NI2OH	55.4	55.4	0.92 (98%)	−73.9

be the electronic properties of the naphthalene ring, as shown in the comparison between pK_a* values for 2NI1OH and 3NI2OH. The oxygen atom electron densities in S_1-N_{anti} and S_1-PT forms of H_2A^{+}* and HA* species are polarized along the long molecular axis (L_b) for 3NI2OH and the short molecular axis (L_a) for 2NI1OH. Therefore, the HA* species of 3NI2OH is comparatively more stable than the corresponding species of 2NI1OH. These observations are in agreement with the computational studies shown below.

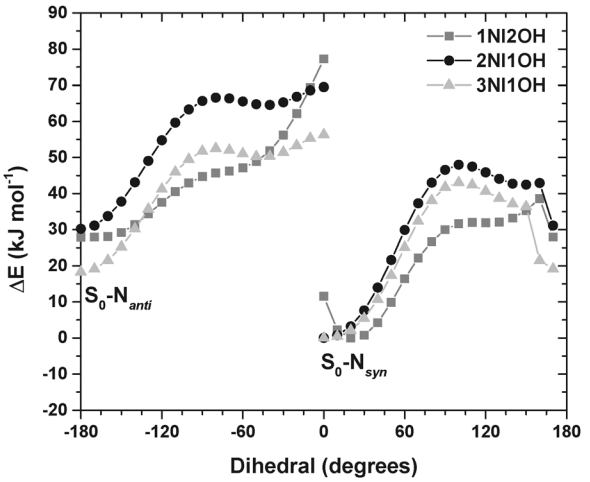

Fig. 5 Potential energy surface in the ground state for the rotation around the interannular bond between the naphthol and the imidazole ring of 1NI2OH, 2NI1OH, and 3NI2OH. Selected structures along the PES are depicted in Fig. S20 of the ESI.†

Computational studies

In order to provide an energy landscape for ESIPT in the *ortho*-(1*H*-imidazol-2-yl)naphthols, as shown in Fig. 4, the minimum-energy reaction path was used to build proton transfer curves in the ground (S_0) and first (S_1) π,π* excited states. The corresponding structures of the N_{syn} and PT forms of either S_0 or S_1 states are also shown in Fig. 4. As established by eqn (4) a negative R_x value in the abscissa indicates the proton is closer to the oxygen than the nitrogen atom while the opposite case results in positive R_x value. In the ground state all compounds share the common feature of a deep well-defined minimum corresponding to the S_0-N_{syn} form, which is always lower in energy compared with the S_0-PT form. Attempts to fully optimize the S_0-PT structure lead back to the S_0-N_{syn} form, indicating that proton transfer is unfavorable in the ground state for all compounds. Table 3 summarizes energy differences obtained from the curves shown in Fig. 4. Activation energy values refer to the difference between energies of the N_{syn} form and transition state structures, which were not fully optimized. Thus, these values are only good estimates of the PT activation energies and a guide for comparing reactivity in the series. The S_0-PT form for 1NI2OH and 2NI1OH occupies a very shallow minimum with computed energy barriers relative to the S_0-N_{syn} form of 31.4 and 32.6 kJ mol^{-1}, respectively. A computed energy barrier of 55.4 kJ mol^{-1} is found for a poorly defined minimum of the S_0-PT form of 3NI2OH. Therefore, GSIPT is almost barrierless and highly favorable for all compounds.

In line with results from absorption studies for 2NI1OH and 3NI2OH, the minimum energy structures obtained along the ground state curves show imidazole and naphthol groups on the same plane. However, the imidazole group for 1NI2OH is rotated by 24.5° out of the naphthalene ring plane due to steric reasons involving the H-8 atom (Fig. 4). As shown in Fig. 5, these structures are true minima in the PES by considering the rotation around the interannular bond between naphthol and imidazole, and thus were used as a common energy point for comparison between the different compounds. Global and local minima for all compounds show intramolecular hydrogen bonds referring to the corresponding S_0-N_{syn} and S_0-N_{anti} forms. Energy profiles are similar except for the relative energy of conformers out of the global minima.

Analysis of the PES profile in Fig. 5 also gives evidences that the lower ground state pK_a values of 2NI1OH relative to its isomers 1NI2OH and 3NI2OH depends on proper geometric requirements for an efficient IMHB. Although 1NI2OH shows a slightly higher energy barrier in going from −180° to zero, overall 2NI1OH exhibits the highest conversion energy from S_0-N_{syn} to S_0-N_{anti} that provides the highest concentration of S_0-N_{syn} conformations with efficiently tuned IMHBs where comparatively the most effective targeting for proton transfer among all isomers is achieved.

Excited state curves of 1NI2OH and 2NI1OH exhibit a double minimum-energy profile corresponding to excited S_1-N_{syn} and S_1-PT forms (Fig. 4). However, 3NI2OH shows a single minimum curve corresponding to the S_1-N_{syn} form. Structural analyses of geometries shown in Fig. 4 reveal that ESIPT occurs in plane for 2NI1OH and 3NI2OH species and out of the plane for 1NI2OH. The excited S_1-N_{syn} form of 1NI2OH exhibits quite a distorted structure with the imidazole group projecting out of the naphthol plane that is also distorted.

Table 4 presents the computed energies at the TD-DFT level showing that our results are in good agreement with the experimental data within deviations of 0.04 to 0.48 eV for the vertical absorption and 0.05 to 0.29 eV for the vertical emission. Actually, the performance of the B3LYP/TZVP calculations is quite satisfactory taking into consideration that the calculations did not include any solvent effect. For example, the agreement with the experimental data for 1NI2OH is comparable with more expensive methods such as CASPT2.

As can be seen in Table 3, energy barriers for proton transfer in the excited state are drastically reduced when compared with

Table 4 TD-DFT (B3LYP/TZVP) computed absorption energies in eV, relative to the ground state energy minimum, for 1NI2OH, 2NI1OH and 3NI2OH[a,b]

Transition[a]	1NI2OH	2NI1OH	3NI2OH
vert (gs → π,π*)	3.77 (*3.73*)	3.93 (*3.45*)[b]	3.62 (*3.52*)
m–m (gs → π,π*)	3.54	3.80	3.42
0–0 (gs → π,π*)	3.43	3.63	3.24
vert (π,π* → gs)	3.11 (*3.06*)	3.31 (*3.02*)	2.42 (*2.47*)
Stokes shift	0.66	0.62	1.20

[a] Vertical (vert), minimum-to-minimum (m–m) and zero-point corrected (0–0) absorption energies. [b] The experimental values, in parenthesis and italic, were obtained at pH 8.0, 6.4 and 7.9 for 1NI2OH, 2NI1OH and 3NI2OH, respectively.

the ground state. Reduction is less for 1NI2OH (32%) due to the energy penalty involved in distorting the molecule in the excited state and about twice as high for 2NI1OH (66%), which suffer negligent torsional effects for conversion of the S_1-N_{syn} form into the S_1-PT form. The largest stabilization of the S_1-PT form is found for 3NI2OH, which also shows a negligible energy barrier for the ESIPT to take place. Two factors are responsible for this effect. First the S_1-N_{syn} form presents proper geometric requirements with both donor and acceptor groups in plane and close contact to each other showing IMHB of only 1.537 Å. Second, the development of an excited ICT state in the S_1-PT form. The ICT state was observed for 2-(2′-hydroxyphenyl)-benzimidazole (HBI)[12e] and is characterized by two large structural changes, the noncoplanarity between the two rings and the piramidalization centered at the C2′ atom of the imidazole ring. These two behaviors are found in the S_1-PT form of 3NI2OH. Piramidalization is defined as the angle between the vector of the interannular bond and the plane formed by the N–C–N atoms of the imidazole ring. The piramidalization angle is 40.3° in the S_1-PT form of 3NI2OH; the corresponding angle for 1NI2OH is only 4.4° and zero for 2NI1OH. The piramidalization angle was 41.5° for 2-(2′-hydroxyphenyl)benzimidazole (HBI) and the pyramidal structure was attributed based on HOMO and LUMO orbitals to an increase of electron density at the corresponding C2′ atom of the benzimidazole ring that repels the atoms bound to it.[12e] This could be an explanation for the piramidalization in 1NI2OH and 3NI2OH, which also show an increase of electron density on the C2′ atom (refer to Fig. S21 in the ESI†). However, the S_1-PT form of 2NI1OH also shows the same behavior, an indication of other effects.

Based on the agreement between the pK_{a1}* values determined by lifetime measurements (Table 1) and the excited state ΔE values obtained by computational studies (Table 3), we can now infer about factors governing the acidity of the H_2A^{+}* species. Although, the determination of accurate pK_{a1}* values is challenging, it may be proposed that the stability of the S_1-PT form rules the acidity of the H_2A^{+}* species. Combination of ESIPT and ICT effects on 3NI2OH provides a low energy S_1-PT form that requires higher HCl concentrations to be protonated. The large ICT effect also decreases the activation energy for the ESIPT process as may be predicted considering the Hammond postulate. On the other hand, the absence of ICT effects in 2NI1OH gives a higher energy S_1-PT structure and also higher activation energy. The 1NI2OH with a noncoplanar ESIPT process shows the S_1-PT with the highest energy and we presume that solvent molecules may be required for the excited state proton transfer to occur. Time-resolved experiments and computation studies are underway to address this point.

The smaller Stokes shift for 2NI1OH (about 80 nm) compared with 3NI2OH (about 150 nm) together with a higher proton transfer barrier for 2NI1OH (Table 3) may seem inconsistent with ESIPT for 2NI1OH. However, the observed Stokes shift for 2NI1OH occurs with OH deprotonation at the L_a-axis, which is weakly associated to excitation at 350 nm and very likely to emission. Besides, 2NI1OH undergoes small structural changes during proton transfer at the excited state. The observation of two bands in acetonitrile (refer to Fig. S19 in the ESI†) is *prima facie* that ESIPT happens, although the emission of S_1-PT is faster in water compared to aprotic solvents and to emission S_1-N_{anti}, which is in fast equilibrium. The pK_a* of −0.95 is also a clear indication of an acid–base equilibrium involving the S_1-PT species.

Conclusions

Taking into consideration the absence of an ICT state for 2NI1OH and the higher ESIPT barrier for 1NI2OH, it is clear that optimal geometric requirements facilitate an ESIPT process, but the final state depends on the electronic configuration of the S_1-PT form. In the case of the *ortho*-(2-imidazolyl)naphthols the ICT state is accessed when both groups involved in the ESIPT process are in the same molecular axis, *i.e.*, the L_b-axis for 3NI2OH.

The IMHB in the ground state, as observed for the first stages of proton transfer in the excited state, are very important for the acidity in the ground state. The highest acidity for the phenol moiety of 2NI1OH compared with its isomers is clearly influenced by proper NACs, which facilitate deprotonation through a strong IMHB between the naphthol hydroxyl group and the neutral imidazole group at the *ortho* position. Moreover, NAC is clearly important for the ESIPT process to take place, but the reactivity of both groups at the excited state very likely decreases the strict structural dependence observed at the ground state.

Experimental section

Materials

Inorganic salts were of analytical grade and were used without further purification. Liquid reagents were purified by distillation. Syntheses of *ortho*-(1*H*-imidazol-2-yl)naphthols **4** were according to a slight modification of the method by Rogers and Bruice (Scheme 6).[26] All synthetic procedures and characterization data for these compounds are presented in the ESI.†

Steady-state optical measurements

UV-Vis and fluorescence spectra were recorded on a Cary 100 spectrophotometer and a Cary Eclipse fluorometer, respectively. Quantum yields for *ortho*-(1*H*-imidazol-2-yl)naphthols (excitation

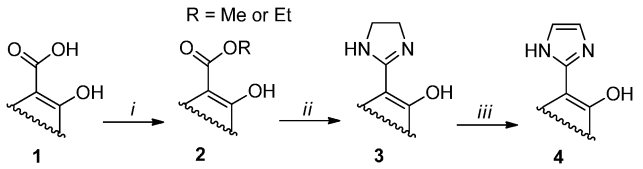

Scheme 6 Synthetic route for preparation of the *ortho*-(1*H*-imidazol-2-yl)naphthols **4**: Conditions: (i) RI, $KHCO_3$, solv. DMF; (ii) ethylenediamine, reflux; (iii) Pd/C 10%, solv. Ph_2O.

at 350 nm) were measured referenced to quinine hemisulfate (QS) monohydrate ($\Phi = 0.546$)[33] in 0.1 M aqueous H_2SO_4 for the sample and the reference. Cuvettes of 3 cm and 1 cm of pathlengths were used to acquire the absorption and emission spectra, respectively (refer to the ESI†).

Time-resolved fluorescence measurements

Decay histograms were obtained using single-photon timing on an Edinburgh Analytical instruments FL 900 spectrofluorometer equipped with a photomultiplier MCM-PMT (Hamamatsu R3809U-50) and a light diode emitting at 335 nm (model EPLED-340), bandwidth of 14.4 nm and temporal detection limit of 815.2 ps. Histograms of the instrument response functions and sample decays were recorded until they typically reached 1×10^4 counts in the peak channel. The decay times were determined by minimizing the reduced chi-square χ^2 for histograms fitted as sums of exponential using Gaussian-weighted nonlinear least-squares fitting.

Titration studies

To a thermostated cell at 25 °C containing 25 mL of 0.01 M HCl, aliquots of 5 mM stock solution of the *ortho*-(1*H*-imidazol-2-yl)naphthols (in 1,4-dioxane) was added to give concentrations of 5.96×10^{-5} M for 1NI2OH and 2.00×10^{-5} M for 2NI1OH and 3NI2OH. The ionic strength was maintained with 0.1 M KCl. Solutions were titrated with small aliquots of aqueous KOH. The pH was continuously measured with a combined glass electrode connected to a digital pH meter calibrated with standard pH solutions. UV-Vis and fluorescence measurements were taken over the pH in quartz cuvettes with optical pathlength of 1 cm and corrected for dilution that was lower than 7.5% of the initial volume. Excitation wavelengths were 330 nm for 1NI2OH and 350 nm for 2NI1OH and 3NI2OH. Acid dissociation constants were calculated using the computer program SQUAD[25] and the spectroscopic data taken at different pH values from near 2 to 12. Standard deviation in the spectroscopic data (σ_{data}), parameters used in the calculations, individual spectra of the species and speciation diagrams are presented in the ESI.† In strong acidic conditions fluorescence intensities and lifetime measurements were recorded at different HCl concentrations from 0.01 to 8 M (pH 2 to H_0 −3.78).[30]

Computational details

The proton transfer curves in the ground and first S_1 excited π,π* states were built using the reaction coordinate proposed by Sobolewski and Domcke:[34]

$$R_x = [r(\mathrm{OH}) - r(\mathrm{NH})]/2 \quad (4)$$

The coordinate-driven minimum-energy path approach was employed in which, for a given value of r(OH), all remaining intramolecular coordinates have been fully optimized in each electronic state, without any symmetry constraint additional frequency calculations were performed at the stationary points located on the proton transfer curves. The geometry optimizations in the ground state were carried out at the Density Functional Theory (DFT)[35] level and the excited state optimizations were carried out using the Time-Dependent Density Functional Theory (TD-DFT).[36] For both cases the hybrid B3LYP[37] functional was used. All geometry optimizations employed the Karlsruhe polarized triple-ζ TZVP basis set.[38] To speed up the calculations, the resolution of the identity approach[39] for the coulomb and the chain of sphere approach[40] for the exchange part of the Fock matrix was used, employing the auxiliary def2-TZVP/J basis sets.[41] The B3LYP functional was chosen because it has been extensively used for the study of intramolecular proton transfer reaction in the ground and excited states, producing satisfactory results.[42] For instance, Aquino, Lischka and Hättig[42d] reported a survey of TD-DFT and RI-CC2 calculations on the excited state potential energy surfaces for ESIPT in several systems and came to the conclusion that the B3LYP functional provides energetic results in agreement with the RI-CC2 method and, for some systems studied, the B3LYP energies agreed very well with CASPT2 and the experimental data. Sobolewski and Domcke[42e] showed that the TD-DFT yields potential surfaces for ESIPT that are essentially parallel to the CASPT2 surfaces. These results encouraged us to use the B3LYP functional in this study. All calculations reported in this work were performed with the ORCA program.[43]

Acknowledgements

We thank the Brazilian Foundations INCT-Catálise, MCT/CNPq, FAPEMIG, Rede Mineira de Química/FAPEMIG, and Pró-Reitoria de Pesquisa da UFMG for their financial support.

References

1 (*a*) T. C. Bruice, *Chem. Rev.*, 2006, **106**, 3119–3139; (*b*) T. C. Bruice, *Acc. Chem. Res.*, 2002, **35**, 139–148; (*c*) T. C. Bruice and F. C. Lightstone, *Acc. Chem. Res.*, 1999, **32**, 127–136.
2 (*a*) F. M. Menger, *Pure Appl. Chem.*, 2005, **77**, 1873–1886; (*b*) F. M. Menger, *Acc. Chem. Res.*, 1985, **18**, 128–134; (*c*) F. M. Menger, *Tetrahedron*, 1983, **39**, 1013–1040.
3 (*a*) M. Garcia-Viloca, J. Gao, M. Karplus and D. G. Truhlar, *Science*, 2004, **303**, 186–195; (*b*) X. Zhang and K. Houk, *Acc. Chem. Res.*, 2005, **38**, 379–385; (*c*) S. Hur and T. C. Bruice, *Proc. Natl. Acad. Sci. U. S. A.*, 2003, **100**, 12015–12020; (*d*) N. A. Khanjin, J. P. Snyder and F. Menger, *J. Am. Chem. Soc.*, 1999, **121**, 11831–11846; (*e*) T. R. Ward, *Angew. Chem., Int. Ed.*, 2008, **47**, 7802–7803.
4 B. S. Souza and F. Nome, *J. Org. Chem.*, 2010, **75**, 7186–7193.
5 (*a*) A. J. Kirby, *Acc. Chem. Res.*, 1997, **30**, 290–296; (*b*) F. Hibbert and J. Emsley, *Adv. Phys. Org. Chem.*, 1990,

26, 255–379; (*c*) F. Hibbert, *Acc. Chem. Res.*, 1984, **17**, 115–120; (*d*) R. Karaman, *Comput. Theor. Chem.*, 2011, **966**, 311–321.

6 A. J. Kirby, *Adv. Phys. Org. Chem.*, 1980, **17**, 183–278.

7 (*a*) E. S. Orth, T. A. S. Brandao, B. S. Souza, J. R. Pliego, B. G. Vaz, M. N. Eberlin, A. J. Kirby and F. Nome, *J. Am. Chem. Soc.*, 2010, **132**, 8513–8523; (*b*) A. J. Kirby, N. Dutta-Roy, D. Silva, J. M. Goodman, M. F. Lima, C. D. Roussev and F. Nome, *J. Am. Chem. Soc.*, 2005, **127**, 7033–7040; (*c*) E. Hartwell, D. R. Hodgson and A. J. Kirby, *J. Am. Chem. Soc.*, 2000, **122**, 9326–9327.

8 (*a*) S. J. Formosinho and L. G. Arnaut, *J. Photochem. Photobiol., A*, 1993, **75**, 21–48; (*b*) P. Wan and D. Shukla, *Chem. Rev.*, 1993, **93**, 571–584; (*c*) B. M. Uzhinov and M. N. Khimich, *Russ. Chem. Rev.*, 2011, **80**, 553–577; (*d*) L. M. Tolbert and K. M. Solntsev, *Acc. Chem. Res.*, 2002, **35**, 19–27; (*e*) J. Z. Zhao, S. M. Ji, Y. H. Chen, H. M. Guo and P. Yang, *Phys. Chem. Chem. Phys.*, 2012, **14**, 8803–8817.

9 J. F. Ireland and P. A. H. Wyatt, *Adv. Phys. Org. Chem.*, 1976, **12**, 131–221.

10 (*a*) H. Shizuka, *Acc. Chem. Res.*, 1985, **18**, 141–147; (*b*) R. F. Grote and J. T. Hynes, *J. Chem. Phys.*, 1980, **73**, 2715–2732.

11 (*a*) B. A. D. Neto, A. A. M. Lapis, E. N. da Silva and J. Dupont, *Eur. J. Org. Chem.*, 2013, 228–255; (*b*) S. J. Lim, J. Seo and S. Y. Park, *J. Am. Chem. Soc.*, 2006, **128**, 14542–14547; (*c*) I. S. K. Kerkines, I. D. Petsalakis, G. Theodorakopoulos and J. Rebek, *J. Phys. Chem. A*, 2011, **115**, 834–840; (*d*) R. M. D. Nunes, M. Pineiro and L. G. Arnaut, *J. Am. Chem. Soc.*, 2009, **131**, 9456–9462.

12 (*a*) F. E. Gostev, L. S. Kol'tsova, A. N. Petrukhin, A. A. Titov, A. I. Shiyonok, N. L. Zaichenko, V. S. Marevtsev and O. M. Sarkisov, *J. Photochem. Photobiol., A*, 2003, **156**, 15–22; (*b*) A. Douhal, F. Amat-Guerri, M. P. Lillo and A. U. Acuña, *J. Photochem. Photobiol., A*, 1994, **78**, 127–138; (*c*) K. Furukawa, N. Yamamoto, T. Nakabayashi, N. Ohta, K. Amimoto and H. Sekiya, *Chem. Phys. Lett.*, 2012, **539**, 45–49; (*d*) H. Konoshima, S. Nagao, I. Kiyota, K. Amimoto, N. Yamamoto, M. Sekine, M. Nakata, K. Furukawa and H. Sekiya, *Phys. Chem. Chem. Phys.*, 2012, **14**, 16448–16457; (*e*) H.-H. G. Tsai, H.-L. S. Sun and C.-J. Tan, *J. Phys. Chem. A*, 2010, **114**, 4065–4079; (*f*) E. L. Roberts, J. Dey and I. M. Warner, *J. Phys. Chem. A*, 1997, **101**, 5296–5301; (*g*) A. Douhal, F. Amat-Guerri, A. Acuna and K. Yoshihara, *Chem. Phys. Lett.*, 1994, **217**, 619–625.

13 A. O. Eseola and N. O. Obi-Egbedi, *Spectrochim. Acta, Part A*, 2010, **75**, 693–701.

14 M. Mosquera, J. C. Penedo, M. C. Ríos Rodríguez and F. Rodríguez-Prieto, *J. Phys. Chem.*, 1996, **100**, 5398–5407.

15 (*a*) A. Douhal, F. Amat-Guerri and A. U. Acuna, *J. Phys. Chem.*, 1995, **99**, 76–80; (*b*) Y. Shigemitsu, T. Mutai, H. Houjou and K. Araki, *J. Phys. Chem. A*, 2012, **116**, 12041–12048; (*c*) T. Mutai, H. Sawatani, T. Shida, H. Shono and K. Araki, *J. Org. Chem.*, 2013, **78**, 2482–2489.

16 The N_{anti} and N_{syn} forms are referred by others as enol forms, while the T_{syn} form is called as keto form. Our nomenclature, following others,[12e] is a tentative of provide a clear distinction between many forms in solution.

17 J. R. Platt, *J. Chem. Phys.*, 1949, **17**, 484–495.

18 P. J. Kovi and S. G. Schulman, *Anal. Chem.*, 1973, **45**, 989–991.

19 J. Catalán, J. C. del Valle, J. Palomar, C. Díaz and J. L. de Paz, *J. Phys. Chem. A*, 1999, **103**, 10921–10934.

20 J. Catalan and J. C. del Valle, *J. Am. Chem. Soc.*, 1993, **115**, 4321–4325.

21 (*a*) C. M. Harris and B. K. Selinger, *J. Phys. Chem.*, 1980, **84**, 891–898; (*b*) C. M. Harris and B. K. Selinger, *J. Phys. Chem.*, 1980, **84**, 1366–1371.

22 D. Huppert, L. M. Tolbert and S. Linares-Samaniego, *J. Phys. Chem. A*, 1997, **101**, 4602–4605.

23 S. Dogra, *J. Mol. Struct.*, 2005, **734**, 51–60.

24 M. Y. Berezin, J. Kao and S. Achilefu, *Chem. – Eur. J.*, 2009, **15**, 3560–3566.

25 D. J. Leggett, S. L. Kelly, L. R. Shiue, Y. T. Wu, D. Chang and K. M. Kadish, *Talanta*, 1983, **30**, 579–586.

26 G. A. Rogers and T. C. Bruice, *J. Am. Chem. Soc.*, 1974, **96**, 2463–2472.

27 A. E. Martell, Z. M. Smith and R. J. Motekaitis, *NIST Critical Stability Constants of Metal Complexes Database Version 8 (for Windows): NIST Standard Reference Database 46*, NIST, Gaithersburg, 2004.

28 Calculated considering a $\Delta pK_a = 2.5$ units and the relationship between ΔG and pK_a, which $\Delta G = 2.303\ RT\ pK_a$.

29 B. S. Souza, Master thesis in Chemistry, Federal University of Santa Catarina, Florianópolis-Brazil, 2008.

30 M. A. Paul and F. A. Long, *Chem. Rev.*, 1957, **57**, 1–45.

31 H. K. Sinha and S. K. Dogra, *Chem. Phys.*, 1986, **102**, 337–347.

32 M. Prémont-Schwarz, T. Barak, D. Pines, E. T. Nibbering and E. Pines, *J. Phys. Chem. B*, 2013, **117**, 4594–4603.

33 W. H. Melhuish, *J. Phys. Chem.*, 1961, **65**, 229–235.

34 A. L. Sobolewski and W. Domcke, *J. Phys. Chem. A*, 1999, **103**, 4494–4504.

35 R. G. Parr and W. Yang, *Density-functional theory of atoms and molecules*, Oxford University Press, New York, 1989.

36 C. Ullrich, *Time-dependent density-functional theory: concepts and applications*, Oxford University Press, New York, 2012.

37 (*a*) A. D. Becke, *J. Chem. Phys.*, 1993, **98**, 5648–5652; (*b*) C. Lee, W. Yang and R. G. Parr, *Phys. Rev.*, 1988, **37**, B785–B789.

38 F. Weigend and R. Ahlrichs, *Phys. Chem. Chem. Phys.*, 2005, **7**, 3297–3305.

39 F. Neese, *J. Comput. Chem.*, 2003, **24**, 1740–1747.

40 F. Neese, F. Wennmohs, A. Hansen and U. Becker, *Chem. Phys.*, 2009, **356**, 98–109.

41 F. Weigend, *Phys. Chem. Chem. Phys.*, 2006, **8**, 1057–1065.

42 (*a*) B. K. Paul and N. Guchhait, *Comput. Theor. Chem.*, 2011, **978**, 67–76; (*b*) B. K. Paul and N. Guchhait, *Comput. Theor. Chem.*, 2011, **972**, 1–13; (*c*) S. Jang, S. I. Jin and C. R. Park, *Bull. Korean Chem. Soc.*, 2007, **28**, 2343; (*d*) A. J. Aquino, H. Lischka and C. Hättig, *J. Phys. Chem. A*, 2005, **109**, 3201–3208; (*e*) A. L. Sobolewski and W. Domcke, *Phys. Chem. Chem. Phys.*, 1999, **1**, 3065–3072.

43 F. Neese, *Wiley Interdiscip. Rev.: Comput. Mol. Sci.*, 2012, **2**, 73–78.